International Journal of Mechanical, Industrial and Aerospace Sciences
ISSN: 2517-9950
Vol:10, No:9, 2016

Linear Dynamic Stability Analysis of a Continuous Rotor-Disk-Blades System

F. Rahimi Dehgolan, S. E. Khadem, S. Bab, M. Najafee

***Abstract*—**Nowadays, using rotating systems like shafts and disks in industrial machines have been increased constantly. Dynamic stability is one of the most important factors in designing rotating systems. In this study, linear frequencies and stability of a coupled continuous flexible rotor-disk-blades system are studied. The Euler-Bernoulli beam theory is utilized to model the blade and shaft. The equations of motion are extracted using the extended Hamilton principle. The equations of motion have been simplified using the Coleman and complex transformations method. The natural frequencies of the linear part of the system are extracted, and the effects of various system parameters on the natural frequencies and decay rates (stability condition) are clarified. It can be seen that the centrifugal stiffening effect applied to the blades is the most important parameter for stability of the considered rotating system. This result highlights the importance of considering this stiffing effect in blades equation.

***Keywords*—**Rotating shaft, flexible blades, centrifugal stiffening, stability.

I. Introduction

ROTATING systems as remarkable machine components are widely used in industrial applications such as turbines, compressors, and aircraft engines. Chang-Jian and Chen [1] studied the dynamic behavior of a flexible rotor supported by porous and non-porous journal bearings. Different non-periodic responses including quasi-periodic and chaotic motions were detected in the dynamic response of the system. The same authors [2], [3] surveyed the rub-impact between the rotor and stator of the aforementioned rotor-bearing model.

Sanches et al. [4] studied a helicopter ground resonance with isotropic and anisotropic multibladed rotor configurations. They employed the Floquet theory for nonlinear dynamic analysis of the system. Also, it was shown that the bifurcation points of the system were dependent on the anisotropic parameters of the system. Santos et al. [5] studied nonlinear phenomena of a coupled rotor-blades system. The system was comprised of a rigid rotor mounted on a flexible foundation and four flexible blades. The blades were modeled using Euler-Bernoulli beam theory. Theoretical results were validated by experimental results for various angular velocities. Chang-Jian [6] studied the dynamic behavior of a gear pair system located on a rotor–bearing system with various strong nonlinear effects containing nonlinear suspension effect, nonlinear couple-stress fluid film force, nonlinear rub-impact force, and nonlinear gear mesh force. Occurrences of the different nonlinear responses such as periodic, sub-harmonic, and chaotic was studied.

Khadem et al. [7] examined the primary resonances of a simply supported in-extensional rotating shaft. The source of the nonlinearity of the shaft was the geometrical nonlinearity and large amplitudes of the vibrations. The multiple scales method was used for the analytical solution. The same authors examined two mode combination resonances in the abovementioned system [8]. Shahgholi et al. [9] investigated free vibration analyses of a nonlinear slender rotating shaft with simply support conditions. Rotary inertia and gyroscopic effect were taken into account to model the system. The forward and backward nonlinear frequencies of the slender rotating shaft were extracted. The same authors [10] surveyed the stability of a rotor system with multi-rigid disk. Multiple scales method was used for analytical analyses. In addition, they investigated the influences of the different system parameters like number of disks, disk mass moment of inertia, rotational speed, external damping, and position of disks on the forward and backward linear frequencies, steady state response, stability, and bifurcations of the system response. They showed that bifurcations happened in the lower speeds by increasing the number of disks. Moreover, it was proved that the response bifurcations occurred in the lower speeds by increasing the number of disks.

Yan et al. [11] studied the dynamic behavior of a flexible rotor on the short journal bearings with nonlinear damping suspension. The equations of motion were solved numerically, and the bifurcation diagrams, orbits, Poincaré maps, and amplitude spectra were used to investigate the system motion. It was proved that the effects of the nonlinear suspension on the stability of the system were dependent on the rotating speed of the rotor. Wang et al. [12] investigated dynamic behaviors of a blade-rotor-bearing system. The blades were modeled as a rotating pendulum and a discrete rotor was located on the journal bearings. Parametric equations of motion were transformed to equations with constant coefficients using the nodal diameter coordinates and periodic transformations. Nonlinear dynamic behaviors of the system were surveyed using the Poincaré maps, three-dimensional spectral plots, and bifurcation diagrams. Zou et al. [13] studied analytically the transverse superharmonic resonances of a marine propulsion shaft under the first blade frequency excitation. The effects of the support stiffness, external load, propeller mass, damping ratio, and slender ratio on the dynamic behavior of the system were surveyed. They showed

F. Rahimi Dehgolan was with the Turbotec-co, Tehran, Iran (corresponding author, phone: +98912-8351163; e-mail: F.rahimi.dehgolaan@gmail.com).

S. E. Khadem, S. Bab, and M. Najafee are with Department of Mechanical Engineering, Tarbiat Modares University, Tehran, Iran (e-mail: khadem@modares.ac.ir, s.bab@modares.ac.ir, m.najafee@gmail.com).

that the nonlinearity in the system behavior decreased by increasing the front and back stern bearings and thrust bearing stiffness. In addition, it was shown that the effects of the middle bearing on the system behavior were negligible.

Genta [14] studied the stability of a rotating blade arrays. An array of rotating pendulums, rigid disk, and dashpot as a suspension were considered to model the system. The stability of the system was investigated considering the effects of the interaction between blades, suspension, and rotating and non-rotating damping. They represented that the system with long blades became unstable in the un-damped in-plane vibration due to the interaction between the blades and suspension.

According to the mentioned researches, the stability analysis of a coupled continuous flexible rotor-disk-blades system has not been yet tried out, while it may achieve notable results. Hence, in this work the linear frequencies and stability of a coupled flexible continuous rotor-disk-blades system has been studied. The Euler-Bernoulli beam theory is used to model the blade and shaft. Considering the gyroscope term of the rotor and the centrifugal stiffing effect applied to the blades for stability analysis of the rotor-disk-blades system is one of the innovations of this work. The equations of motion are obtained using the extended Hamilton principle. The Coleman and complex transformations are employed to simplify the equations of motion. The natural frequencies of the linear part of the system are obtained, and the effects of the different system parameters on the frequencies and decay rates (stability condition) of the system are investigated.

II. Modeling and Derivation of Equations

Fig. 1 depicts a rotor system comprised of a rotating shaft, a disk, and blades that are located at ($x = x_d$) position of the shaft. The shaft and blades are modeled as flexible beams for which rotary inertia is considered, but shear deformation is omitted. The following coordinates are considered to study the dynamics of the system:

1) The X-Y-Z frame, as an inertial coordinate system.
2) The x-y-z local frame attached to the principal axes of the deformed shaft cross section.

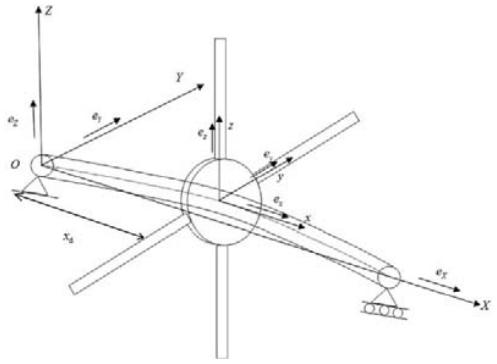

Fig. 1 Inertial and local coordinates for the continuous rotor-disk-blades system

To obtain the equations of motion, the extended Hamilton principle is employed as:

$$\delta \int_0^t (T - V)dt = 0 \tag{1}$$

where T, V, δ and t are the kinetic energy, potential energy, variational operator, and time, respectively. The kinetic and potential energy of different components of the system are:

$$T = T_{\text{Shaft}} + T_{\text{Disk}} + T_{\text{Blades}} + T_{\text{im}}, V = V_{\text{Shaft}} + V_{\text{Blades}} \tag{2}$$

where $T_{\text{Shaft}}, T_{\text{Disk}}$, and T_{Blades} are the kinetic energy of the shaft, disk and blades, respectively. Also V_{Shaft} and V_{Blades} are the potential energy of the shaft and blades, respectively. Also, T_{im} is related to dynamic imbalances or mass eccentricity of the shaft. These terms are obtained in the following sections.

B. The Kinetic and Potential Energy of the Rotating Shaft

Use The displacements of the rotating shaft are nominated by variables $u(x,t)$, $v(x,t)$, and $w(x,t)$, where these variables are the deflections of the shaft in an arbitrary location *x* in the *X*, *Y*, and *Z* directions, respectively. The transformation between the original frame *X-Y-Z* and the local frame *x-y-z* is described by three successive Euler's angles $\psi(x,t)$, $\theta(x,t)$, and $\beta(x,t)$ (Fig. 2) [7] $\psi(x,t)$ and $\theta(x,t)$ are due to the shaft bending, and $\phi(x,t)$ is related to the torsional deformation; moreover, $\beta(x,t)$ is the torsional rigid body rotation of the shaft about *x* -axis, which can be demonstrated as:

$$\beta(x,t) = \Omega t + \phi(x,t) \tag{3}$$

where Ω is the rotational speed of the rotor.

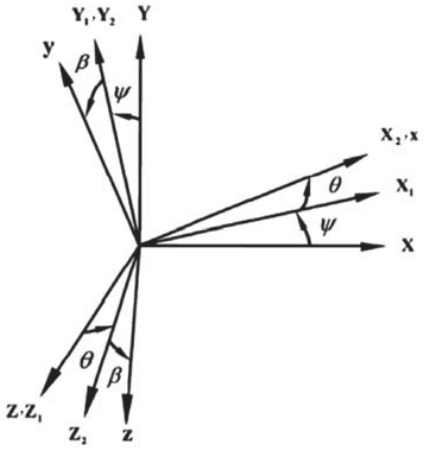

Fig. 2 Transformation between inertial and local coordinates using Euler's angles [7]

The angular velocities ω_1, ω_2, ω_3 and curvatures k_1, k_2

and k_3 of the rotating shaft can be extracted by the Euler angles. Hence, the angular velocities and curvatures of the shaft can be represented as [15]:

$$\omega_1=(\dot{\phi}+\Omega-\dot{\psi}\sin\theta),\ \omega_2=(\dot{\psi}\sin\phi\cos\theta+\dot{\theta}\cos\phi),\quad \omega_3=(\dot{\psi}\cos\phi\cos\theta-\dot{\theta}\sin\phi) \tag{4}$$

$$k_1=(\phi'-\psi'\sin\theta),\ k_2=(\psi'\sin\phi\cos\theta+\theta'\cos\phi),\quad k_3=(\psi'\cos\phi\cos\theta-\theta'\sin\phi) \tag{5}$$

where prime and dot denote differentiation with respect to the x and t, respectively. Thus, the kinetic and potential energies of the rotating shaft can be written as:

$$T_{\text{shaft}}=\frac{1}{2}\int_0^l\left(m(\dot{u}^2+\dot{v}^2+\dot{w}^2)+I_1\omega_1^2+I_2\omega_2^2+I_3\omega_3^2\right)dx \tag{6}$$

$$V_{\text{shaft}}=\frac{1}{2}\int_0^l(N_{11}\alpha^2+D_{11}k_1^2+D_{22}k_2^2+D_{33}k_3^2)\,dx \tag{7}$$

where m, l, I_1, I_2, I_3, N_{11}, D_{11}, D_{22}, D_{33} and α are the mass per unit length of the shaft, length of shaft, polar mass moment of inertia, mass moment of inertia about y-axis, mass moment of inertia about z-axis, longitudinal stiffness, torsional stiffness, flexural stiffness about y-axis, flexural stiffness about z-axis, and strain along the neutral axis of the shaft, respectively, which can be determined as:

$$\begin{aligned}&I_{11}=\int(y^2+z^2)dm\ ,\ I_{22}=\int z^2\,dm\ ,\ I_{33}=\int y^2\,dm\\&D_{11}=\int_A G(y^2+z^2)dA,\ D_{22}=\int_A Ez^2dA\ ,\ N_{11}=\int_A EdA\\&\alpha=\sqrt{(1+u')^2+v'^2+w'^2}-1\ ,\ D_{33}=\int_A Ey^2dA\end{aligned} \tag{8}$$

It is worthy to note that I_{22}=I_{33} and D_{22}=D_{33} for a circular shaft. The kinetic energy due to dynamic imbalances of the shaft is as [7]:

$$T_{\text{im}}=\frac{1}{2}\int_0^l\begin{pmatrix}m\Omega^2\left[e_y^2(x)+e_z^2(x)\right]dx\\-2m\Omega\begin{pmatrix}\left[\dot{v}e_z(x)+\dot{w}e_y(x)\right]\sin\Omega t\\+\left[\dot{v}e_y(x)-\dot{w}e_z(x)\right]\cos\Omega t\end{pmatrix}\end{pmatrix}dx \tag{9}$$

where $e_y(x)$ and $e_z(x)$ are mass eccentricity distributions with respect to the y and z-axes, respectively.

C. The Kinetic Energy of the Disk

The disk is supposed to be rigid and is located at the middle of the shaft; its potential energy is zero and the kinetic energy is obtained as:

$$T_{\text{disk}}=\left(m_{\text{disk}}(\dot{u}^2+\dot{v}^2+\dot{w}^2)+J_{\text{disk}}\omega_1^2+I_{\text{disk}}(\omega_2^2+\omega_3^2)\right)\delta(x-x_d) \tag{10}$$

where m_{disk}, J_{disk}, I_{disk} and δ(x) are mass of the disk, polar mass moment of inertia of the disk, diametrical mass moment of inertia of the disk, and the Dirac delta function.

D. The Kinetic and Potential Energies of the Blades

With the aim of analyzing the dynamics of the blades, a local coordinate is considered described by x_b, y_b, z_b. Its y_b axis is along the radial direction of disk and blades; its z_b axis is in disk plane and perpendicular to blades and its x_b axis is perpendicular to y_b and z_b axes. Based on Fig. 1, the position vector of an arbitrary particle on the i-th blade is obtained as:

$$\mathbf{R}_{(\text{beam})_i}=\begin{Bmatrix}x_d+u(x_d,t)\\v(x_d,t)\\w(x_d,t)\end{Bmatrix}+\begin{bmatrix}\cos\phi_1(x_d,t)&-\sin\phi_1(x_d,t)&0\\\sin\phi_1(x_d,t)&\cos\phi_1(x_d,t)&0\\0&0&1\end{bmatrix}\begin{bmatrix}1&0&\theta(x_d,t)\\0&1&0\\-\theta(x_d,t)&0&1\end{bmatrix}\begin{bmatrix}1&0&0\\0&1&-\psi(x_d,t)\\0&\psi(x_d,t)&1\end{bmatrix}\begin{Bmatrix}x_b\\\Lambda_i(\varsigma,t)+z_b\\r+\varsigma\end{Bmatrix} \tag{11}$$

where r, ς, Λ_i, x_b and y_b are disk radius, distance of the particle from the base of the blade, the amplitude of vibration of the i-th blade, and the location of the particle on the cross section of the blade, respectively. Furthermore, x_d is the longitudinal position of the disk on the rotor. $\psi(x_d,t)$, $\theta(x_d,t)$ and $\phi_1(x_d,t)$ are the Euler angles of the rotor that are calculated at the attachment position of the disk related to the i-th blade. The $\phi_1(x_d,t)$ is:

$$\phi_1(x_d,t)=\Omega t+\phi(x_d,t)+\nu_i \tag{12}$$

In (12) is the angle between i-th blade and 1-th blade, which is obtained as:

$$\nu_i=\frac{2\pi(i-1)}{n}\qquad i=1,...,n \tag{13}$$

Using (11)-(13), the kinetic energy of the i-th blade is extracted as:

$$\begin{aligned}T_{(\text{blade})_i}&=\frac{1}{2}m'\int_0^{l'}\int_{A'}\dot{\mathbf{R}}_{(\text{blade})_i}.\dot{\mathbf{R}}_{(\text{blade})_i}\,dA'dx=\frac{m'A'l'}{2}\left(\dot{w}^2+\dot{v}^2+\dot{u}^2\right)+\frac{m'A'}{2}\int_0^{l'}\dot{\Lambda}_i^2d\varsigma-\\&\frac{m'A'}{2}(\Omega+\dot{\phi})^2\int_0^{l'}\Lambda_i^2d\varsigma-\frac{m'I'_{11}r}{2}(\Omega+\dot{\phi})^2+\frac{m'A'\Gamma_3}{2}(\Omega+\dot{\phi})^2+m'A'\Gamma_3\left(\dot{\psi}(\Omega+\dot{\phi})\theta\right)+\\&m'A'\Gamma_2(\Omega+\dot{\phi})\int_0^{l'}\dot{\Lambda}_id\varsigma-\frac{m'A'I'_{33}\Gamma_2}{8l'}(\Omega+\dot{\phi})^2+m'A'\Gamma_2\sin\phi_1\left(-\dot{w}(\Omega+\dot{\phi})+\dot{w}\psi+\dot{u}(\Omega+\dot{\phi})\theta\right)\\&+m'A'\sin\phi_1\left(-\dot{w}\int_0^{l'}\dot{\Lambda}_id\varsigma-(\Omega+\dot{\phi})\dot{v}\int_0^{l'}\Lambda_id\varsigma\right)+m'A'\Gamma_2\cos\phi_1\left(\dot{v}(\Omega+\dot{\phi})+\dot{u}(\Omega+\dot{\phi})\psi-\dot{u}\dot{\theta}\right)+\\&m'A'\cos\phi_1\left(\dot{v}\int_0^{l'}\dot{p}_id\varsigma-(\Omega+\dot{\phi})\dot{w}\int_0^{l'}\Lambda_id\varsigma\right)+\frac{m'A'\Gamma_3}{2}\left(\dot{\theta}\cos\phi_1-\dot{\psi}\sin\phi_1\right)^2,\ q=0,...,n-1\end{aligned} \tag{14}$$

It should be mentioned that the blades are positioned on the disk at $(x=x_d)$ point of the rotor; therefore, (14), $\dot{\psi}$, $\dot{\theta}$, $\dot{u}$, $\dot{v}$, $\dot{w}$, and $\dot{\phi}$ are calculated at this location. Furthermore, A', m', and l' are the cross sectional area, mass density, and the length of the blade, respectively. I_{11} is the second moment of area of the cross section of the blade about axis parallel with

the rotor. Γ_2 and Γ_3 in (14) are obtained as:

$$\Gamma_2 = \int_0^{l'} (r+\varsigma)\mathrm{d}\varsigma,\ \Gamma_3 = \int_0^{l'} (r+\varsigma)^2 \mathrm{d}\varsigma \tag{15}$$

The potential energy of the i-th blade is:

$$V_{(\text{blade})_i} = \frac{1}{2}\int_0^{l'} EI'_{11}\left(\frac{\mathrm{d}^2\Lambda_i(\varsigma,t)}{\mathrm{d}\varsigma^2}\right)^2 \mathrm{d}\varsigma \tag{16}$$

Therefore, the total kinetic and potential energy of the blades are:

$$T_{\text{Blades}} = \sum_{i=1}^{n} T_{(\text{blade})_i},\ V_{\text{Blades}} = \sum_{i=1}^{n} V_{(\text{blade})_i} \tag{17}$$

E. In-Extensionality Assumption

In (7), the strain along the neutral axis of the shaft (α) is $\alpha = \sqrt{(1+u')^2+v'^2+w'^2}-1$. It is assumed that one of the supports (right support in Fig. 1) can move along the longitudinal axis; hence, strain along the neutral axis of the shaft can be neglected ($\alpha = 0$) [15]. Therefore, one has:

$$u' = \sqrt{1-v'^2-w'^2}-1 = -\frac{1}{2}(v'^2+w'^2)+\cdots \tag{18}$$

In addition, the shaft is supposed to be slender; hence, the angles ψ and θ have the following relations with the linear displacement of the shaft [7]:

$$\psi = \sin^{-1}\frac{v'}{\sqrt{(1+u')^2+v'^2}},\quad \theta = \sin^{-1}\frac{-w'}{\sqrt{(1+u')^2+v'^2+w'^2}} \tag{19}$$

In addition, the main torsional frequency is much higher than the main flexural frequency in the slender shafts; therefore, the torsional inertia terms can be neglected compared to the flexural inertia and stiffness terms [16]. Also, if $v = O(\varepsilon)$, and $w = O(\varepsilon)$, where ε is a small dimensionless parameter, the nonlinearities would be of $O(\varepsilon^4)$ in the torsional equation of motion; thus, one has:

$$\phi = -\int_0^x v''w'dx + \ldots \tag{20}$$

Accordingly, equations of motion are extracted employing (1) to (20) and the extended Hamilton principle as:

$$\left[m'A'\ddot{\Lambda}_i + C_{\text{blade}}\dot{\Lambda}_i + EI'_{11}\frac{\mathrm{d}^4\Lambda_i}{\mathrm{d}\varsigma^4}\right] + \left[-m'A'(\Omega+\dot{\phi})^2\Lambda_i + m'A'(r+\varsigma)\ddot{\phi} + m'A'(r+\varsigma)(\Omega+\dot{\phi})^2\frac{\mathrm{d}\Lambda_i}{\mathrm{d}\varsigma}\right.$$
$$\left. -\frac{m'A'}{2}(\Omega+\dot{\phi})^2\left((r+l')^2-(r+\varsigma)^2\right)\frac{\mathrm{d}^2\Lambda_i}{\mathrm{d}\varsigma^2}\right] + \left[m'A'\ddot{v}\delta(x-x_d)\cos\phi_i - m'A'\ddot{w}\delta(x-x_d)\sin\phi_i\right] = 0 \qquad i = 1\ldots N_b \tag{21}$$

$$\left[m\left(\ddot{v}+\frac{v'}{2}\int_0^x(\dot{v}'^2+\ddot{v}'v'+\dot{w}'^2+\ddot{w}'w')dx + \frac{v''}{2}\int_l^x\int_0^x(\dot{v}'^2+\ddot{v}'v'+\dot{w}'^2+\ddot{w}'w')dxdx\right) + c\dot{v} - I_1\Omega\ddot{w}' - I_2\ddot{v}'' + D\left(v'^2v^{(IV)}+\right.\right.$$
$$\left.\left. v'w^{(IV)}w' + 3w'''w''v' + v''w''^2 + v''^3 + w'''v''w' + 4v'v''v'''\right)\right] +$$
$$\left[m_{\text{disk}}\left(\ddot{v}\delta(x-x_d) + \frac{v'\delta(x-x_d)}{2}\int_0^{x_d}(\dot{v}'^2+\ddot{v}'v'+\dot{w}'^2+\ddot{w}'w')dx + \frac{v''\delta(x-x_d)}{2}\int_l^{x_d}\int_0^{x_d}(\dot{v}'^2+\ddot{v}'v'+\dot{w}'^2+\ddot{w}'w')dxdx\right)\right.$$
$$\left. -J_{\text{disk}}\Omega\ddot{w}'\delta(x-x_d) - I_{\text{disk}}\ddot{v}''\delta(x-x_d)\right] +$$
$$\left[\delta(x-x_d)\sum_{i=1}^{N_b}\left(m'A'l'\ddot{v} + m'A'\Gamma_3((\Omega+\dot{\phi})w')' - m'A'\sin\phi_i\left(\ddot{\phi}\int_0^{l'}\Lambda_i d\varsigma + 2(\Omega+\dot{\phi})\int_0^{l'}\dot{\Lambda}_i d\varsigma + \Gamma_2(\Omega+\dot{\phi})^2 + \Gamma_2\ddot{w}'\right)\right.\right.$$
$$-m'A'\cos\phi_i\left((\Omega+\dot{\phi})^2\int_0^{l'}\Lambda_i d\varsigma - \Gamma_2\ddot{\phi} - \int_0^{l'}\ddot{\Lambda}_i d\varsigma - \Gamma_2\dot{u}'(\Omega+\dot{\phi}) - \Gamma_2\dot{u}\dot{\phi}' - \Gamma_2\dot{w}'(\Omega+\dot{\phi})\right) +$$
$$\left.\left. m'A'\Gamma_3\left(\ddot{v}''\sin^2\phi_i + \left(\dot{v}''(\Omega+\dot{\phi}) - \ddot{w}''\right)\sin 2\phi_i - \left(2(\Omega+\dot{\phi})\dot{w}''\right)\cos 2\phi_i\right)\right)\right] - \left[m\Omega^2\left(e_z(x)\cos\Omega t - e_y(x)\sin\Omega t\right)\right] = 0 \tag{22}$$

$$\left[m\left(\ddot{w}+\frac{w'}{2}\int_0^x(\dot{v}'^2+\ddot{v}'v'+\dot{w}'^2+\ddot{w}'w')dx+\frac{w''}{2}\int_l^x\int_0^x(\dot{v}'^2+\ddot{v}'v'+\dot{w}'^2+\ddot{w}'w')dxdx\right)+c\dot{w}+I_1\Omega\ddot{v}'-I_2\ddot{w}''+D\left(w''v''^2\right.\right.$$
$$\left.\left.+v'v'''w''+3w'v''v'''+w'v'v^{(IV)}+w'^2w^{(IV)}+w''^3+4w'w''w'''\right)\right]$$
$$+\left[m_{\text{disk}}\left(\ddot{w}\delta(x-x_{\text{d}})+\frac{w'\delta(x-x_{\text{d}})}{2}\int_0^{x_{\text{d}}}(\dot{v}'^2+\ddot{v}'v'+\dot{w}'^2+\ddot{w}'w')dx+\frac{w''\delta(x-x_{\text{d}})}{2}\int_l^{x_{\text{d}}}\int_0^{x_{\text{d}}}(\dot{v}'^2+\ddot{v}'v'+\dot{w}'^2+\ddot{w}'w')dxdx\right)+\right.$$
$$\left.J_{\text{disk}}\Omega\ddot{v}'\delta(x-x_{\text{d}})-I_{\text{disk}}\ddot{w}''\delta(x-x_{\text{d}})\right] \tag{23}$$
$$+\left[\delta(x-x_{\text{d}})\sum_{i=1}^{N_{\text{b}}}\left(m'A'l'\ddot{w}-m'A'\Gamma_3\left((\Omega+\dot{\phi})\dot{v}'\right)'+m'A'\sin\phi_i\left(-\Gamma_2\ddot{\phi}+\Gamma_2\ddot{v}'-\int_0^{l'}\ddot{\Lambda}_i d\varsigma+(\Omega+\dot{\phi})^2\int_0^{l'}\Lambda_i d\varsigma\right.\right.\right.$$
$$\left.-\Gamma_2\dot{u}'\dot{\phi}-\Gamma_2\dot{u}\dot{\phi}'-\Gamma_2\dot{u}'(\Omega+\dot{\phi})\right)+m'A'\cos\phi_i\left(-\Gamma_2(\Omega+\dot{\phi})^2+\Gamma_2\dot{v}'(\Omega+\dot{\phi})-2(\Omega+\dot{\phi})\int_0^{l'}\dot{\Lambda}_i d\varsigma-\ddot{\phi}\int_0^{l'}\Lambda_i d\varsigma+\Gamma_2\ddot{u}'\pi\right)+$$
$$\left.\left.m'A'\Gamma_3\left(\ddot{w}''\cos^2\phi_i+\left(\frac{\ddot{v}''}{2}-\dot{w}''(\Omega+\dot{\phi})\right)\sin 2\phi_i+\left(\dot{v}''(\Omega+\dot{\phi})\right)\cos 2\phi_i\right)\right)\right]-\left[m\Omega^2\left(e_{\text{z}}(x)\sin\Omega t+e_{\text{y}}(x)\cos\Omega t\right)\right]=0$$

Equation (21) is the equation of motion of the blades and (22) and (23) are equations of motion of the rotor in the Y and Z axes, respectively. To be more understandable for the readers, the terms are divided in a few brackets based on their nature in the aforementioned equations. In (21), the terms are separated in three brackets that are relevant to the blade structure, the effect of rotor torsional vibration on the blade vibration, and the effect of rotor lateral vibration on the blade vibration, respectively. In (22) and (23), the terms are grouped into four brackets that are related to the rotor structure, the effects of the mass and mass moment of inertias of the disk on the lateral vibration of the rotor, the effects of the mass, mass moment of inertia and vibration of the blades on the lateral vibration of the rotor, and the mass eccentricity force of the rotor, respectively.

The direction of viscous damping forces applied to the rotating shaft and blades is opposite of the shaft and blades velocities direction; therefore, the damping force $C_{\text{blade}}\dot{\Lambda}_{\text{i}}$, $c\dot{v}$ and $c\dot{w}$ are added to (21), (22) and (23), respectively, where C_{blade} and c are damping coefficients of the rotor and blade, respectively.

III. Transformations

The analytical analysis of the large number of the motion equations is quite complicated and almost impossible; hence, to reduce the number of equations of motion, the Coleman and complex transformations are employed. Two parameters η and ξ are used in the Coleman transformation as [4]:

$$\eta=\frac{-2}{N_{\text{b}}}\sum_{i=1}^{N_{\text{b}}}\Lambda_{\text{i}}(\varsigma,t)\sin\phi_i,\quad \xi=\frac{-2}{N_{\text{b}}}\sum_{i=1}^{N_{\text{b}}}\Lambda_{\text{i}}(\varsigma,t)\cos\phi_{\text{i}} \tag{24}$$

It is worthy to note that the Coleman transformation [4], the nodal diameter coordinates of the blades [12] and the multi-blade coordinate (MBC) transformation [17] have the same nature. Also, in order to transform the equations of motion to a complex plane, the following parameters are exploited:

$$p=\xi-\text{j}\eta,\ z=v+\text{j}w,\ \bar{p}=\xi+\text{j}\eta,\ \bar{z}=v-\text{j}w \tag{25}$$

where $\text{j}^2=-1$. Using these transformations, $2+N_b$ equations of motion (21)-(23) are transformed to two equations of motions as:

$$\left[\left(m(\ddot{z}+\frac{z'}{2}\int_0^x(2\dot{z}'\dot{\bar{z}}'+\ddot{z}'\bar{z}'+\ddot{\bar{z}}'z')dx+\frac{z''}{2}\int_1^x\int_0^x(2\dot{z}'\dot{\bar{z}}'+\ddot{z}'\bar{z}'+\ddot{\bar{z}}'z')dxdx)\right)+c\dot{z}+\text{j}\Omega I_1\dot{z}''-I_2\ddot{z}''\right.$$
$$\left.+D\left(z^{IV}+2z''z'\bar{z}'''+\frac{1}{2}z''\bar{z}'z'''+\frac{3}{2}\bar{z}''z'z'''+\bar{z}''z''^2+\frac{1}{2}z^{(IV)}\bar{z}'z'+\frac{1}{2}\bar{z}^{(IV)}z'^2\right)\right]+$$
$$\left[\left(m_{\text{disk}}+m'A'l'N_b\right)\left(\ddot{z}\delta(x-x_d)+\delta(x-x_d)\frac{z'}{2}\int_0^{x_d}(2\dot{z}'\dot{\bar{z}}'+\ddot{z}'\bar{z}'+\ddot{\bar{z}}'z')dx+\delta(x-x_d)\frac{z''}{2}\int_1^{x_d}\int_0^{x_d}(2\dot{z}'\dot{\bar{z}}'+\ddot{z}'\bar{z}'+\ddot{\bar{z}}'z')dxdx\right)\right. \tag{26}$$
$$\left.+\text{j}\Omega(J_{\text{disk}}+m'A'N_{\text{p}}\Gamma_3)\dot{z}''\delta(x-x_{\text{d}})-(I_{\text{disk}}+\frac{m'A'N_p\Gamma_3}{2})\dot{z}''\delta(x-x_d)\right]$$
$$+\left[\frac{m'A'N_{\text{p}}}{2}\delta(x-x_d)\int_0^{l'}\ddot{p}d\varsigma\right]-\left[\Omega^2\left(\text{j}e_z(x)+e_{\text{y}}(x)\right)\text{e}^{\text{j}\Omega t}\right]=0$$

$$[m'A'\ddot{p}+c_{\text{blade}}\dot{p}+EI_{11}\frac{\mathrm{d}^4p}{\mathrm{d}\varsigma^4}]+[-2m'A'(\Omega+\dot{\phi})^2p-2m'A'(\Omega+\dot{\phi})\mathrm{j}\dot{p}-m'A'\ddot{\phi}\mathrm{I}p-c_{\text{blade}}(\Omega+\dot{\phi})\mathrm{j}p+m'A'(r+\varsigma)(\Omega+\dot{\phi})^2\frac{\mathrm{d}p}{\mathrm{d}\varsigma}$$
$$-\frac{m'A'}{2}(\Omega+\dot{\phi})^2\{(r+l')^2-(r+\varsigma)^2\}\frac{\mathrm{d}^2p}{\mathrm{d}\varsigma^2}]+[m'A'\ddot{z}\delta(x-x_d)]=0 \quad (27)$$

where ϕ, $\dot{\phi}$, $\ddot{\phi}$ are:

$$\phi=\frac{\mathrm{j}}{4}\int_0^{x_d}\left((z''+\bar{z}'')(z'-\bar{z}')\right)\mathrm{d}x,\ \dot{\phi}=\frac{\mathrm{j}}{4}\int_0^{x_d}\left((\dot{z}''+\dot{\bar{z}}'')(z'-\bar{z}')+(z''+\bar{z}'')(\dot{z}'-\dot{\bar{z}}')\right)\mathrm{d}x,\ \ddot{\phi}=\frac{\mathrm{j}}{4}\int_0^{x_d}\left((\ddot{z}''+\ddot{\bar{z}}'')(z'-\bar{z}')+2(\dot{z}''+\dot{\bar{z}}'')(\dot{z}'-\dot{\bar{z}}')+(z''+\bar{z}'')(\ddot{z}'-\ddot{\bar{z}}')\right)\mathrm{d}x \quad (28)$$

IV. Nondimensionalized Equation

In order to perform the analytical analysis, the following dimensionless parameters are applied to the equations of motion:

$$p^*=\frac{p}{l},z^*=\frac{z}{l},e^*_y=\frac{e_y}{l},e^*_y=\frac{e_y}{l},x^*=\frac{x}{l},x^*_{\mathrm{d}}=\frac{x_{\mathrm{d}}}{l},\mathrm{i}=\sqrt{-1},$$
$$\Omega^*=\Omega\sqrt{\frac{m_rl^4}{D}},t^*=t\sqrt{\frac{D}{ml^4}},c^*_{\text{blade}}=\frac{c_{\text{blade}}}{m'A'}\sqrt{\frac{m_rl^4}{D}},c^*_r=\frac{c_rl^2}{\sqrt{m_rD}},I^*_2=\frac{I_2}{m_rl^2}, \quad (29)$$
$$I^*_1=\frac{I_1}{m_rl^2},R_{\mathrm{I1}}=\frac{J_{\text{disk}}+m'A'n_{bl}\Gamma_3}{m_rl^3},R_{\mathrm{I2}}=\frac{I_{\text{disk}}+\frac{m'A'n_{bl}\Gamma_3}{2}}{m_rl^3},$$
$$R_{\mathrm{ml}}=\frac{m_{\text{disk}}+m'A'l'n_{bl}}{m_rl},R_{\mathrm{m2}}=\frac{m'A'l'n_{bl}}{2m_rl},I'^*_{11}=\frac{EI'_{11}m_rl^4}{m'A'Dl'^4},r^*_d=\frac{r_d}{l'},\varsigma^*=\frac{\varsigma}{l'}$$

Thus, the following dimensionless equations of motion can be obtained using these terms:

$$[(\ddot{z}^*+\frac{z'^*}{2}\int_0^{x^*}(2\dot{z}'^*\dot{\bar{z}}'^*+\ddot{z}'^*\bar{z}'^*+\ddot{\bar{z}}'^*z'^*)\mathrm{d}x^*+\frac{z''^*}{2}\int_1^{x^*}\int_0^{x^*}(2\dot{z}'^*\dot{\bar{z}}'^*+\ddot{z}'^*\bar{z}'^*+\ddot{\bar{z}}'^*z'^*)\mathrm{d}x^*\mathrm{d}x^*)+c^*_r\dot{z}^*+\mathrm{i}\Omega^*I^*_1\dot{z}'^*-I^*_2\dot{z}''^*+(z^{IV*}+2z''^*z'^*\bar{z}''^*+$$
$$\frac{1}{2}z''^*\bar{z}'^*z''^*+\frac{3}{2}\bar{z}''^*z'^*z'''^*+\bar{z}''^*z''^{*2}+\frac{1}{2}z^{(IV)^*}\bar{z}'^*z'^*+\frac{1}{2}\bar{z}^{(IV)^*}z'^{*2})]+[R_{\mathrm{ml}}(\ddot{z}^*\delta(x-x^*_{\mathrm{d}})+\delta(x-x^*_{\mathrm{d}})\frac{z'^*}{2}\int_0^{x^*_{\mathrm{d}}}(2\dot{z}'^*\dot{\bar{z}}'^*+\ddot{z}'^*\bar{z}'^*+\ddot{\bar{z}}'^*z'^*)\mathrm{d}x+ \quad (30)$$
$$\delta(x^*-x^*_{\mathrm{d}})\frac{z''^*}{2}\int_1^{x^*_{\mathrm{d}}}\int_0^{x^*_{\mathrm{d}}}(2\dot{z}'^*\dot{\bar{z}}'^*+\ddot{z}'^*\bar{z}'^*+\ddot{\bar{z}}'^*z'^*)\mathrm{d}x^*\mathrm{d}x^*)+\mathrm{i}\Omega^*R_{\mathrm{I1}}\delta(x^*-x^*_{\mathrm{d}})\dot{z}''^*-R_{\mathrm{I2}}\delta(x^*-x^*_{\mathrm{d}})\ddot{z}''^*]+[R_{\mathrm{m2}}\delta(x^*-x^*_{\mathrm{d}})\int_0^1\ddot{p}\mathrm{d}\varsigma^*]-[\Omega^{*2}(\mathrm{i}e_z(x^*)+e_y(x^*))\mathrm{e}^{\mathrm{i}\Omega^*t^*}]=0$$

$$[\ddot{p}^*+c_{\text{blade}}\dot{p}^*+I'^*_{11}\frac{\mathrm{d}^4p^*}{\mathrm{d}\varsigma^{*4}}]+[-2(\Omega^*+\dot{\phi}^*)^2p^*-2(\Omega^*+\dot{\phi}^*)\mathrm{i}\dot{p}^*-(\Omega^*+\dot{\phi}^*)\dot{\mathrm{i}}p^*- \quad (31)$$
$$c^*_{\text{blade}}(\Omega^*+\dot{\phi}^*)\mathrm{i}p^*+(r^*_d+\varsigma^*)(\Omega^*+\dot{\phi}^*)^2\frac{\mathrm{d}p^*}{\mathrm{d}\varsigma^*}-\frac{(\Omega^*+\dot{\phi}^*)^2}{2}\{(r^*_d+1)^2-(r^*_d+\varsigma^*)^2\}\frac{\mathrm{d}^2p^*}{\mathrm{d}\varsigma^{*2}}]+[\ddot{z}^*\delta(x^*-x^*_{\mathrm{d}})]=0$$

V. Galerkin Method

The equations of motion of the system are dependent on time and the position. Upon utilization the Galerkin method, the equations would be dependent only on time [18]. The rotor shaft and blades are modeled as the free-free and clamped-free beams, respectively. Therefore, the standard mode shapes of the rotor and blades are used for the Galerkin method. Consequently, these mode shapes can be written as:

$$\phi_{\mathrm{i}}(x^*)=\sin i\pi x^*,0<x^*<1,i=1,2,... \quad (32)$$

$$\psi_{\mathrm{i}}(\varsigma^*)=\{\sin(\beta_il'\varsigma^*)-\sinh(\beta_il'\varsigma^*)\}-$$
$$\frac{(\sin(\beta_il')+\sinh(\beta_il'))}{(\cos(\beta_il')+\cosh(\beta_il'))}.\{\cos(\beta_il'\varsigma^*)-\cosh(\beta_il'\varsigma^*)\} \quad (33)$$
$$\beta_1l'=1.8751,\beta_2l'=4.6941,\beta_3l'=7.8548,...,\quad 0\langle\varsigma^*\langle1$$

Displacements of the rotor and blades are discretized to time and the position employing the following relations:

$$z^*(x^*,t^*)=\sum_{i=1}^{n}\phi_{\mathrm{i}}(x^*)q_{zi}(t),n\geq1,\ p^*(\varsigma^*,t)$$
$$=\sum_{i=1}^{m}\psi_{\mathrm{i}}(\varsigma^*)q_{bi}(t),m\geq1 \quad (34)$$

where n and m are the number of rotor and blades mode shapes that are utilized in the Galerkin method, respectively.

VI. Analytical Analysis (Linear)

The linear coupled nondimensional motion equations of the system are acquired by keeping the linear terms of the equations of motion of the system ((30) and (31)) as:

$$\ddot{z}^*+c^*_r\dot{z}^*+\mathrm{i}\Omega^*I^*_1\dot{z}''^*-I^*_2\ddot{z}''^*+z^{IV*}+R_{\mathrm{ml}}\ddot{z}^*\delta(x-x^*_{\mathrm{d}})+$$
$$\mathrm{i}\Omega^*R_{\mathrm{I1}}\delta(x^*-x^*_{\mathrm{d}})\dot{z}''^*-R_{\mathrm{I2}}\delta(x^*-x^*_{\mathrm{d}})\ddot{z}''^*+ \quad (35)$$
$$R_{\mathrm{m2}}\delta(x^*-x^*_{\mathrm{d}})\int_0^1\ddot{p}\mathrm{d}\varsigma^*=0$$

$$\ddot{p}^* + c_{\text{blade}}\dot{p}^* + I_{11}^{r*}\frac{\mathrm{d}^4 p^*}{\mathrm{d}\varsigma^{*4}} - 2\Omega^{*2}p^* - 2\Omega^* \mathrm{i}\dot{p}^* - c_{\text{blade}}^*\Omega^* \mathrm{i}p^* + \ddot{z}^*\delta(x^* - x_{\text{d}}^*) + (r_d^* + \varsigma^*)\Omega^{*2}\frac{\mathrm{d}p^*}{\mathrm{d}\varsigma^*} - \frac{\Omega^{*2}}{2}\{(r_d^* + 1)^2 - (r_d^* + \varsigma^*)^2\}\frac{\mathrm{d}^2 p^*}{\mathrm{d}\varsigma^{*2}} = 0 \quad (36)$$

Equation (35) is the linear equation of motion of the rotor. In (35), the terms are related to the mass inertia of the rotor, the damping of the rotor shaft, the gyroscopic effect of the rotor (generated by the polar mass moment of inertia), the effect of diametrical moment of inertia of the rotor, stiffness of the rotor, the mass inertia of the disk and blades (like an added mass effect in fluid-structure phenomena [19]), the effect of the gyroscopic moment of the disk and blades on the rotor, the effect of diametrical moment of inertia of the disk and blades on the rotor, and the effects of vibrations of the blades on the rotor, respectively. Also, (36) is the linear equation of motion of the blades array. In this equation, the terms are relevant to the mass inertia of the blades, the damping of the blades, the stiffness of the blades, the spin softening effect [20], Coriolis acceleration, the rotating damping, and the effect of the rotor vibration on the blades (like a base excitation [21]), respectively. Two last terms are related to the centrifugal stiffening effect in the rotating structure [22]. These equations ((35) and (36)) can be compared to (54) of [14] that focuses on a discrete model of rotor, disk, and blades array assembly. Indeed, one of the superiority of this paper over [14] is considering the gyroscope term of the rotor and the centrifugal stiffening effect applied to the blades. On the other hand, in (54) of [14], the term related to the spin softening effect was $\Omega^2(\frac{r}{l}-1)$ (Ω, r, and l were rotational speed, disk radius, and length of the pendulums), respectively. In [14] it was shown that the sign of this phrase determined the stability condition of the system. For short ($l<r$ or $(\frac{r}{l}-1)>0$) and long pendulums ($l>r$ or $(\frac{r}{l}-1)<0$), system was stable and unstable, respectively. It should be noted that the blades were modeled as pendulum in the discrete model of the reference [14]. In the present work, which the blades are modeled using Euler-Bernoulli beam theory, the related term is $-2\Omega^{*2}$. The reason of this difference from a mathematical point of view is that the spin softening term for the rotating pendulum, string, and blades are positive, negative, and negative, respectively. This is visible by considering (6), (36), and (54) of chapter 13 of [22]. Conceptually, when the rotary pendulum oscillates in the centrifugal force field, this force helps the move to continue. In contrast, if the cross-section or particle of the rotating string or beam vibrates in the centrifugal force field, this force will prevent moving and will undermine the stiffness force of the beam and string.

VII. Numerical Examples

To analyze the natural frequencies in detail, the Campbell diagram of the system is plotted. At first, the stiffness of the blades and the damping of rotor and blades are not taken into account to draw diagram. For validation of the obtained Campbell diagram with Fig. 4 of [14], the gyroscopic term of the rotor and centrifugal stiffening effect (that are innovation of this work) applied to the blades are neglected in the first plot.

For obtaining the natural frequencies of the system, firstly, the Galerkin method is applied to (35) and (36), and the coupled ordinary differential equations of the system are extracted. Then, the characteristic equation of the system is obtained using the system equations in matrix form and calculating determinant of them [21]. The characteristic equation of the system is a four degree polynomial; therefore, it has four roots. These roots have real and imaginary parts that are natural frequency and decay rate, respectively. If the decay rate of one of the modes is positive, the system will be unstable.

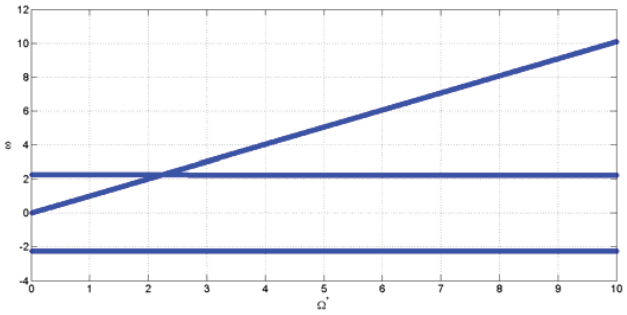

Fig. 3 Campbell diagram (natural frequencies) of the rotor, disk, and blades assembly without considering the stiffness of the blades, the damping of rotor and blades, the gyroscopic term of the rotor, and centrifugal stiffening effect of the blades for $l'/r_d = 5$

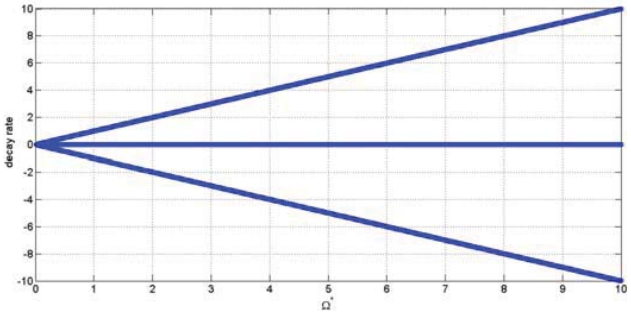

Fig. 4 Campbell diagram (decay rates) of the rotor, disk, and blades assembly without considering the stiffness of the blades, the damping of rotor and blades, the gyroscopic term of the rotor, and centrifugal stiffening effect of the blades for $l'/r_d = 5$

To have a detailed insight, without considering the stiffness of the blades, the damping of rotor and blades, the gyroscopic term of the rotor, and centrifugal stiffening effect applied to the blades, the system has at least one unstable mode in all rotational speeds for different ratios of the blade length and disc radius (long and short blade) in any case. Figs. 3 and 4

show, respectively, natural frequencies and decay rates of the rotor, disk, and blades assembly as a function of the rotational speed without considering the stiffness of the blades, the damping of rotor and blades, the gyroscopic term of the rotor, and centrifugal stiffening effect applied to the blades for $l'/r_d=5$. As it is clear in Fig. 4, since decay rate of one of modes is positive in all speeds, system is unstable in any speeds. As it was noted, in this case, for different ratios of the blade and disc length, the Campbell diagrams of the system are qualitatively the same as Figs. 3 and 4. The decay rate diagram is not changed significantly by adding the gyroscopic term of the rotor, and system still has an unstable mode. Fig. 5 depicts the natural frequencies of the rotor, disk, and blades assembly as a function of the rotational speed without considering the stiffness of the blades, the damping of rotor and blades, and centrifugal stiffening effect of the blades fo $l'/r_d=5$. It is obvious that the dependency of the natural frequencies to the rotational speed increases by considering the gyroscopic term of the rotor.

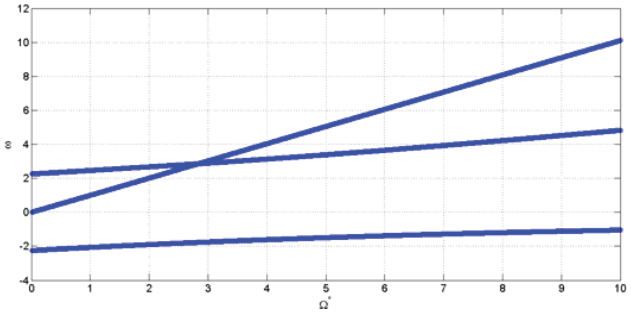

Fig. 5 Campbell diagram (natural frequencies) of the rotor, disk, and blades assembly without considering the stiffness of the blades, the damping of rotor and blades, and centrifugal stiffening effect of the blades for $l'/r_d=5$

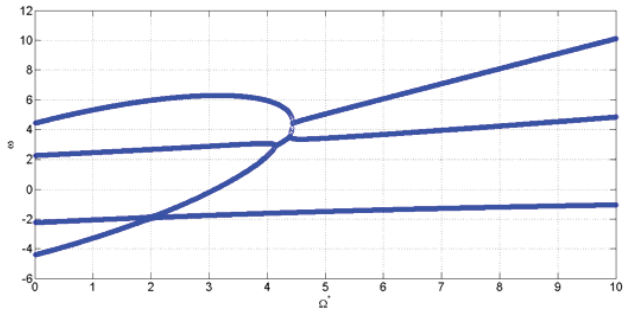

Fig. 6 Campbell diagram (natural frequencies) of the rotor, disk, and blades assembly without considering the damping of rotor and blades and centrifugal stiffening effect of the blades for $l'/r_d=5$

Figs. 6 and 7 demonstrate natural frequencies and decay rates of the rotor, disk, and blades assembly as a function of the rotational speed without considering the damping of rotor and blades and centrifugal stiffening effect for $l'/r_d=5$. Comparing Fig. 6 to Fig. 5 shows that the natural frequency related to the blade at zero rotational speed increases by shifting the stiffness of the blades from zero to 4.5 (nondimensional). Also, comparing Fig. 4 to Fig.7 proves that the range of instability is changed to higher rotational speeds $(\Omega^*>4.2)$ for $l'/r_d=5$ by considering the stiffness of the blades. Fig. 6 depicts that the system has four frequencies. Two of them are about 2.1 and 4.3 related to the rotor and blade at rest $(\Omega^*=0)$. The investigations show that in this case, the unstable region existed for all of the blades and rotor length ratio, but if the blades become shorter, their natural frequencies will increase; hence, the difference between blades and rotor natural frequencies will become greater. Accordingly, the interaction between the blade and rotor frequencies and instability occur at higher rotational velocities. Fig. 8 shows natural frequencies of the rotor, disk, and blades assembly as a function of the rotational speed without considering the damping of rotor and blades and centrifugal stiffening effect applied to the blades for $l'/r_d=3$. The coalescence of frequencies and emergence of the instability occur at $(\Omega^*=10.4)$. For instance, the range of the instability for the shorter blade $(l'/r_d=0.7)$ is obtained as $(\Omega^*>220)$. This means that the system with a shorter blade becomes unstable at higher rotational speeds.

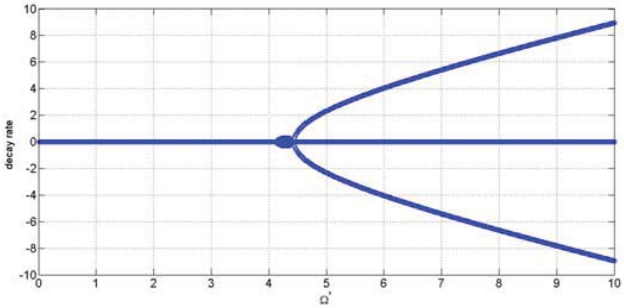

Fig. 7 Campbell diagram (decay rates) of the rotor, disk, and blades assembly without considering the damping of rotor and blades and centrifugal stiffening effect of the blades for $l'/r_d=5$

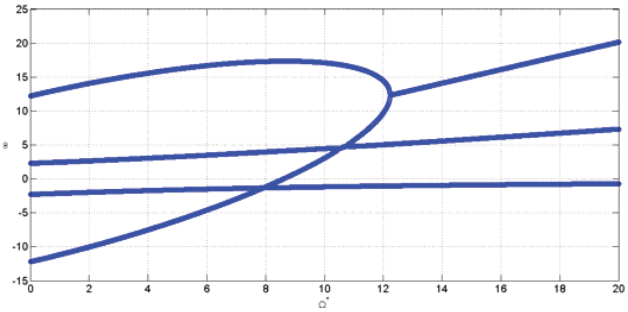

Fig. 8 Campbell diagram (natural frequencies) of the rotor, disk, and blades assembly without considering the damping of rotor and blades and centrifugal stiffening effect of the blades for $l'/r_d=3$

Fig. 9 represents natural frequencies of the rotor, disk, and

blades assembly as a function of the rotational speed without considering the damping of rotor and blades for $l'/r_d = 5$. Further analyses show that decay rates for all modes of the system are zero in this case and for different blade to rotor length ratio (short and long blade). In fact, the system with different length blades is dynamically stable by considering the centrifugal stiffening effect applied to the blades. The computations indicate that the normal magnitude of the rotor and blades damping without considering the centrifugal stiffening effect of the blades cannot eliminate instability. With the centrifugal stiffening effect, the decay rates decrease from zero to a negative value by considering damping for the rotor and blades (Fig. 10). Of course, we know that the normal amount of damping slightly affects the natural frequency values. Finally, we can say that the determining parameter for stability condition of the rotor, disk, blades system is the centrifugal stiffening effect applied to the blades, and it indicates the importance of considering the centrifugal stiffening in the corresponding mathematical modeling.

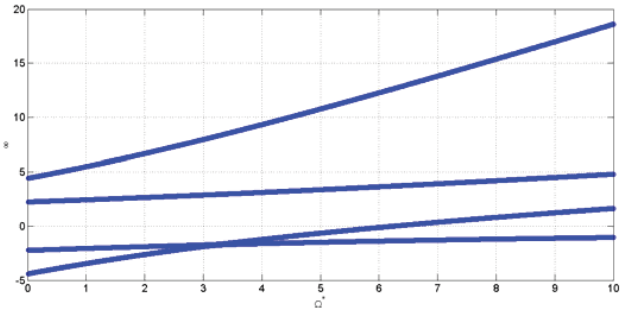

Fig. 9 Campbell diagram (natural frequencies) of the rotor, disk, and blades assembly without considering the damping of rotor and blades for $l'/r_d = 5$

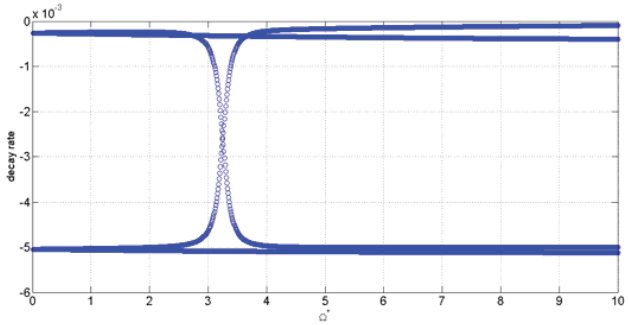

Fig. 10 Campbell diagram (decay rates) of the rotor, disk and blades for $l'/r_d = 5$ and $c_r^* = c_{\text{blade}} = 0.01$

VIII. Conclusions

The linear frequencies and stability of the coupled continuous flexible rotor-disk-blades system have been studied. The Euler-Bernoulli beam theory has been used to model the blade and shaft. The equations of motion have been obtained using the extended Hamilton principle. The Coleman and complex transformations have been utilized to simplify the equations of motion. The natural frequencies of the linear part of the system have been extracted, and the dependency of the frequencies and decay rates (stability condition) to various parameters of the system have been investigated. The most important result of this work can be represented as:

- By considering blades as a pendulum in the rotor-disk-blade system [14] the sign of the spin softening term is different from its sign in cases the blades are modeled as a continuous beam (this work); hence, the stability condition of the system changes.
- The dependency of the natural frequencies to the rotational speed increases by considering the gyroscopic term of the rotor, but the instability condition of the system remains constant.
- The rotating system with different length blades is dynamically stable by considering centrifugal stiffening effect of the blades. Therefore, we can say that the determining parameter for stability of the rotor, disk, blades system is the centrifugal stiffening applied to the blades.

References

[1] C. W. Chang-Jian, C. K. Chen, "Chaotic response and bifurcation analysis of a flexible rotor supported by porous and non-porous bearings with nonlinear suspension," Nonlinear Analysis: Real World Applications, 10 (2009) 1114–1138.
[2] C. W. Chang-Jian, C. K. Chen, "Chaos and bifurcation of a flexible rub-impact rotor supported by oil film bearings with nonlinear suspension," Mechanism and Machine Theory, 42 (2007) 312–333.
[3] C. W. Chang-Jian, C. K. Chen, "Chaos of rub–impact rotor supported by bearings with nonlinear suspension," Tribology International, 42 (2009) 426–439.
[4] Sanches L, Michon G, Berlioz A, Alazard D, "Instability zones for isotropic and anisotropic multibladed rotor configurations," Mechanism and Machine Theory, 46 (2011) 1054–1065.
[5] Santos IF, Saracho CM, Smith JT, Eiland J, "Contribution to experimental validation of linear and non-linear dynamic models for representing rotor–blade parametric coupled vibrations," Journal of Sound and Vibration, 271 (2004) 883–904.
[6] C. W. Chang-Jian, "Bifurcation and chaos of gear-rotor–bearing system lubricated with couple-stress fluid," Nonlinear Dynamic, 79(1) (2015) 749-763.
[7] S. E. Khadem, M. Shahgholi, S. A. A. Hosseini, "Primary resonances of a nonlinear in-extensional rotating shaft," Mechanism and Machine Theory, 45 (2010) 1067–1081.
[8] S. E. Khadem, M. Shahgholi, S. A. A. Hosseini, "Two-mode combination resonances of an in-extensional rotating shaft with large amplitude," Nonlinear Dynamic, 65 (2011) 217–233.
[9] Shahgholi M, Khadem S. E. and Bab S., "Free vibration analysis of a nonlinear slender rotating shaft with simply support conditions," Mechanism and Machine Theory, 82 (2014) 128-140.
[10] Shahgholi M, Khadem S. E. and Bab S., "Nonlinear vibration analysis of a spinning shaft with multi-disks," Meccanica, 50(9) (2015) 2293-2307.
[11] S. Yan, E. H. Dowell, B. Lin, "Effects of nonlinear damping suspension on nonperiodic motions of a flexible rotor in journal bearings," Nonlinear Dynamic, 78(2) (2014) 1435-1450.
[12] L. Wang, D. Q. Cao, W. Huang, "Nonlinear coupled dynamics of flexible blade–rotor–bearing systems," Tribology International, 43 (2010) 759–778.
[13] D. Zou, Z. Rao, N. Ta, "Coupled longitudinal-transverse dynamics of a marine propulsion shafting under superharmonic resonances," Journal of Sound and Vibration, 346 (2015) 248–264.
[14] Genta, G., "On the stability of rotating blade arrays," Journal of Sound and Vibration, 273(4–5) (2004) 805-836.
[15] Nayfeh, A. H. and P. F. Pai, "Linear and nonlinear structural mechanics," 2004, New York: Wiley-Interscience.

[16] Nayfeh, A. H., "Introduction to perturbation techniques," 2011, John Wiley & Sons.
[17] Staino A., B. Basu, and S. R. K. Nielsen, "Actuator control of edgewise vibrations in wind turbine blades," Journal of Sound and Vibration, 2012. 331(6): p. 1233-1256.
[18] L. Meirovitch, "Fundamentals of Vibrations," McGraw Hill, New York, 2001.
[19] Parviz Ghadimi, Hadi Paselar Bandari, Ali Bankhshandeh Rostami, "Determination of the heave and pitch motions of a floating cylinder by analytical solution of its diffraction problem and examination of the effects of geometric parameters on its dynamics in regular waves," International Journal of Applied Mathematical Research, 1(4) (2012) 611-633.
[20] S. W. Shaw, B. Geist, "Tuning for performance and stability in systems of nearly Tautochronic torsional vibration absorbers," J. Vibr. Acoust, 132 (2010) 041005 (-1).
[21] W Thomson, "Theory of Vibration with Applications," GEORGE ALLEN & UNWIN, London, 1981.
[22] G. Genta, "Dynamics of Rotating Systems," springer, (2005).